ELECTRICAL CONDUCTIVITY IN 3D: COUPLING MASS FLOW, TEMPERATURE AND HYDRAULIC RADIUS

Supti Sadhukhan*

Keywords: Electrical conductivity, temperature, reactive transport, numerical modelling

This study delves into the intricate relationship between Peclet number, pore throat size, and temperature on the electrical conductivity of fluid-filled straight channels in three dimensions, employing simulation techniques. Results revealed a quadratic increase in conductance with porosity under steady-state conditions across all Peclet number ranges examined. Conductivity remained constant with porosity for each Peclet number. The rate of increase in conductivity diminished with Peclet number. Non-linear increases in conductivity were observed with temperature in transient cases, with a threshold temperature marking the onset of conductivity. Conductivity experienced augmentation with the observation time throughout the temperature range considered. In the linear regime, conductivity showed a linear rise with temperature, although the rate of increase dwindled with elapsed time suggesting conductivity attains saturation at steady state.

*Corresponding Author
E-Mail: suptisadhukhan@gmail.com
Department of Physics, Jogesh Chandra Chaudhuri College,
Kolkata 700033, India.

DOI: 10.17628/ecb.2018.8

1 Introduction

The electrical conductivity of fluids is crucial for various industrial processes and environmental applications.Electrical conductivity measurements are essential in industrial processes where the presence of conductive substances in a solution needs to be monitored. This measurement is particularly valuable in applications where the type of conductive substance is irrelevant, such as in ultra-pure water treatment for semiconductor manufacturing, or where specific conductive substances need to be controlled, like in brine solutions for salinity control. In the context of wastewater treatment, electrical conductivity plays a vital role in determining the level of dissolved substances, chemicals, and minerals in the water. Monitoring electrical conductivity helps in selecting the appropriate treatment processes to remove contaminants and impurities effectively. This is crucial for preserving the environment, protecting public health, and ensuring the quality of water for various purposes. Electrical conductivity is used as a proxy for salinity in bodies of water, where higher conductivity indicates a higher concentration of dissolved salts or ions. This property is utilized in environmental monitoring, aquaculture, and water treatment to assess water quality and salinity levels. Fluid conductivity can serve as a tool to identify specific groundwater flow paths within the subsurface. By analyzing conductivity data along with other information, such as temperature corrections, specific conductance, and composition-dependent coefficients, it becomes possible to trace groundwater flow paths accurately. The conductivity of a liquid is influenced by the presence and concentration of charged particles or electrolytes dissolved in the liquid, such as ions from salts, acids, bases, or other substances. The more free ions present, the higher the conductivity of the fluid [1]. Conductivity measurements can also be influenced by changes in temperature, as the mobility of ions in the liquid may vary with temperature. Conductivity data are often paired with temperature compensations to ensure accurate readings. Conductivity measurements can be used to estimate total dissolved solids concentration in certain cases, and for bodies of water, conductivity is used as a proxy for salinity. Magnetic flow meters and conductive level switches require a minimum level of conductivity in the liquid to function properly, as they rely on the liquid's ability to carry an electrical current.

Conductivity measurements play a pivotal role in the analysis and interpretation of electrical resistivity logging in wellbores [2, 3, 4] , as well as in interpreting electrical resistivity image data [5, 6]. Electrical resistivity tomography has been employed to model the transport of solutes and

electrical current flow in petrophysical contexts [7]. Various theoretical methodologies have emerged for modeling the electrical conductivity of fractal porous media [8, 9]. Dalla et al. [10] applied finite-difference discretization to ascertain the effective resistivity of porous media at the pore scale.

Researchers face the challenge to apply lab findings on ionic fluid flow in rocks to real-world situations. Labs use small samples, and scaling those results to vast rock formations can be inaccurate. This study aims to bridge the gap between lab and real-world scenarios by examining flow of ionic fluids in porous rocks under two conditions: transient and steady flow. In transient flow, electrodes measure the conductance as soon as the fluid enters the rock. In the case for steady flow, due to the small sample size, the fluid passes through the entire pore space quickly and resulting in steady concentration of the emerging plume. The objective here is to explore the governing principles underlying the conductivity's growth concerning temperature, porosity, and the Peclet number, and the circumstances when the results from these two contrasting scenarios (transient and steady) align.

2 Methodology

Straight channels of varying widths and of the same length are generated. Fluid flow is achieved by solving Navier-Stokes equation. The ionic distribution can be obtained in two ways -(i) solving the Advection Diffusion Equation (ADE) directly (ii) transporting the ions by TDRW method which is obtained from ADE equation. Both these ways have been used. Given a ionic distribution, conductance is solved using Laplace's equation.

2.1 Structure Generation

Three dimensional straight channels of varying widths and equal lengths are discretized into cubical cells. The channels are encased within a rock except at the inlet and outlet. Increasing channel width increases the porous volume. This implies channel width is directly proportional to porosity(ϕ).

2.2 Electrical Conductance

The pore cells are attributed a conductance proportional to the number of ions in it as per the ionic distribution obtained through solving ADE. In the pore cells that have no ions, a false conductance ~ 0.001 is introduced to implement to the Laplace's equation. As the ionic concentration is significantly high at the inlet, the introductions of the false conductance contributes negligibly to the effective conductance. It is assumed that the value of the conductance is the same throughout the cell. The equivalent conductance of any two adjacent pore cells with individual conductance values g_1 and g_2 is represented as $g_{12} = g_1 g_2/(g_1 + g_2)$. The method adopted for solving the electrical conductivity is broadly taken from [11] A pair of imaginary electrodes are applied at the inlet and outlet of the channels which serve as the boundary conditions. To implement this condition, a single layer of cells is introduced at these positions, with potentials $V_{in} = 1$ and $V_{out} = 0$ assigned to them, respectively. The potentials of the pore cells are iterated as per Eq.(1) until convergence is achieved. The potential of a pore cell *i* is updated from the potentials and conductance values of its six nearest neighbour cells. Convergence implies steady state at which the current flowing, I_{steady} through the cross section at any position of the sample is the same throughout. If node *i* is an internal node, the solution of V_i is given by Eq.(1) where *j* runs over all the 6 nearest neighbour cells in three-dimensions.

$$V_i = \frac{\sum_{j=1}^{j=6} g_{ij} V_j}{\sum_{j=1}^{j=6} g_{ij}} \quad (1)$$

Following Ohm's law, the effective electrical conductance is $G = I_{steady} / (V_{in} - V_{out})$. In this study, $V_{in} - V_{out}$ is unity, which yields $G \equiv I_{steady}$.

2.3 Fluid Flow and Transport of Ions

To solve for fluid flow, a constant pressure head is maintained with no-slip boundary conditions enforced at the pore-rock interface of the channel [12, 13]. The fluid flow is described by the Navier-Stokes equation. In this study, the simplified form of the Navier-Stokes equation is used assuming inertial term to be negligible and absence of external forces.

$$\frac{\partial \mathbf{v}}{\partial t} = -\frac{1}{\rho}\nabla p + \eta \nabla^2 \mathbf{v} \quad (2)$$

The simplified Navier-Stokes equation (Eq.2) coupled with the equation of continuity (Eq.3) enables the system to attain steady state.

$$\nabla . \mathbf{v} = 0 \quad (3)$$

In this study, transport of ions have been implemented through two ways both of which are equivalent. For the study of G-ϕ, the Advection Diffusion Equation (ADE) is applied directly (Eq.4) for transportation of the ions. In the subsequent investigation, the Time Domain Random Walk (TDRW) mechanism which is derived from Eq.4 is used for movement of the ions.

$$\frac{\partial C}{\partial t} + \boldsymbol{\nabla}.(\mathbf{v}\mathrm{C}) - \boldsymbol{\nabla}.D\,\boldsymbol{\nabla}\mathrm{C} = 0 \qquad (4)$$

In this equation C refers to concentration, D represents diffusivity and V is the velocity of fluid. The Time Domain Random Walk (TDRW) mechanism is involves random walkers which mimic the role of ions. The time taken for a walker to leap from one pore cell to an adjacent pore cell depends on the local velocity of the cell in which it resides. The distance travelled in each leap remains constant which is equal to the length of the cubical pores. The detailed mechanism is discussed in few papers [14, 15].

Discretization of Eq.(4) in 3-D yields

$$\begin{aligned}\frac{\partial C_i}{\partial t} = &-\frac{u}{h}\left[C_i - C_{up_x}\right] - \frac{v}{h}\left[C_i - C_{up_y}\right] \\ &- \frac{w}{h}\left[C_i - C_{up_z}\right] \\ &+ \frac{D}{h^2}\left[C_{dn_x} + C_{up_x} - 2C_i\right] \\ &+ \frac{D}{h^2}\left[C_{dn_y} + C_{up_y} - 2C_i\right] \\ &+ \frac{D}{h^2}\left[C_{dn_z} + C_{up_z} - 2C_i\right]\end{aligned} \qquad (5)$$

C_i refers to the concentration at the i^{th} pixel. C_{upx} and C_{dnx} denote the concentration values at the pixels adjacent to *i* along x axis. The same idea is extrapolated for C_{upy} and C_{dny} and C_{upz} and C_{dnz} for y axis and z axis. The distance between two adjacent pixels is represented by *h*. Velocity **v** is resolved into components *u*, *v* and *w* along the x,y and z axes respectively. Rearrangement of the terms of equation (Eq.5) yields

$$\frac{\partial C_i}{\partial t} = -C_i \sum_j b_{j,i} + \sum_j C_j\, b_{i,j} \qquad (6)$$

where,

$$b_{up_x,i} = b_{up_y,i} = b_{up_z,i} = b_{i,dn_x} = b_{i,dn_y} = b_{i,dn_z} = \frac{D}{h^2}$$

$$b_{dn_x,i} = b_{i,up_x} = \frac{D}{h^2} + \frac{u}{h}$$

$$b_{dn_y,i} = b_{i,up_y} = \frac{D}{h^2} + \frac{v}{h}$$

$$b_{dn_z,i} = b_{i,up_z} = \frac{D}{h^2} + \frac{w}{h}$$

The transition probability P_{ij} for any transition between neighbours, say from *j* to *i*, and the corresponding time taken is denoted as

$$P_{ij} = \frac{b_{ij}}{\sum_j b_{ij}} \qquad (7)$$

$$T_j = \frac{1}{\sum_j b_{ij}} \qquad (8)$$

Temperature of the fluid impacts the viscosity of the fluid, which subsequently affects the mobility of the ions. The effect of changing temperature is integrated in the transition time through a weighting factor, depending on the corresponding viscosity. The weighting factor is given by the ratio of a reference viscosity and the viscosity pertaining to the concerned temperature. This weighting actor is multiplied with the transition time of a ion in a pixel as mentioned in the previous section. Lower the viscosity, higher is the mobility and thereby lower is the residence time of an ion in a pore pixel.

3 Results and Discussion

The first part of the study involved the study of *G* and σ with $\phi(w)$ for different Peclet number *Pe* as shown in Fig.1. Widths of channels considered were of the order: 15,19,23,27,31,35 pixels, and the length was 250 pixels.In this study, 1 pixel= $\Delta x = 5 \times 10^{-4}$ cm.The inlet concentration of ions was fixed at 500. The ADE is implemented directly to obtain the concentration profile in the sample after obtaining the velocity distribution as given by the Navier-Stokes equation. The concentration profile corresponds to the steady state distribution which implies that there is no change in the concentration of the emerging plume from the outlet. In this simulation, the individual conductance, *g*, of each pore cell is considered numerically equal to the concentration of the cell. Laplace solution gives *G* from the *g* distribution. The effective electrical conductivity is obtained using the relation $\sigma = \frac{GL}{A}$ from *G*.

It was observed that *G* has a wide response to *Pe* (Fig.1a). At the lowest Peclet number, *Pe* = 1,

there is no significant change in *G* with increasing pore throat (w). Increasing *Pe* from 5 to 100, showed increase in *G* with w quadratically, following the relation $y = ax^2+bx+c$ (Table 1). The overall behaviour of the plots reveal that there is rapid change in *G* with increase in *Pe* until about *Pe* = 50 beyond which it tends to saturate (Fig.2).

The conductivity is almost constant for all channel widths (Fig.1b). Increasing *Pe* implies higher concentration distribution and consequently higher σ values. The slight depression with increasing width is possibly due to finite size effects.

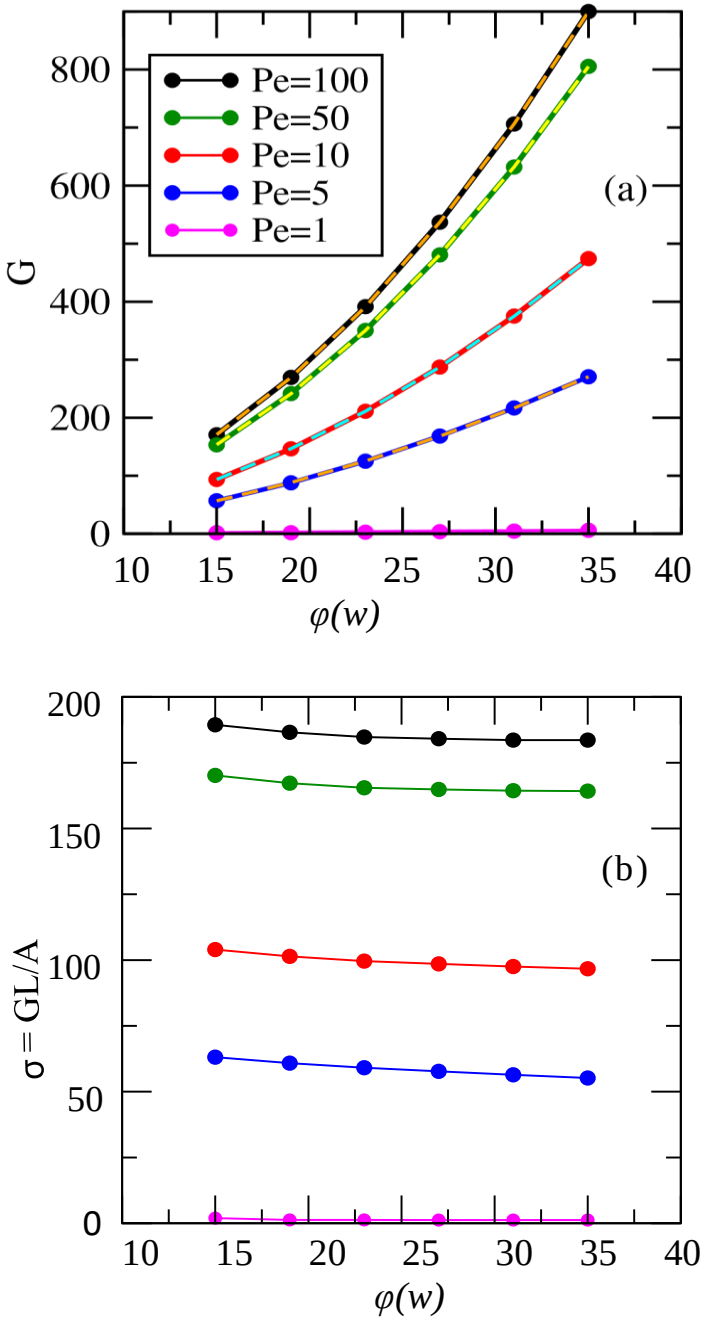

Figure 1: Fluid flow at different *Pe* through a channel of tuned width w. Solid lines denote *G* while the dotted lines represent the quadratic fit. (a) *G* verses ϕ(w). (b)σ verses ϕ(w).

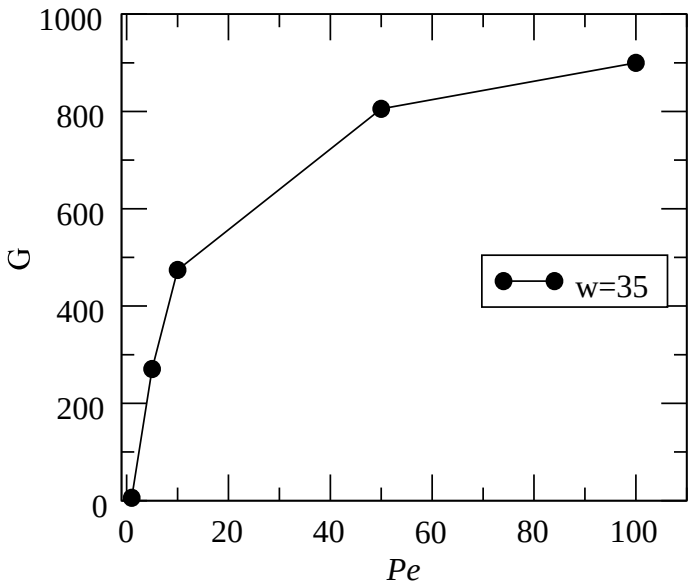

Figure 2: Non-linear growth of *G* with *Pe* for w=35.

Table 1: Quadratic fit of G- ϕ plots

Pe	***a***	***b***	***c***
1	0.007	-0.167	2.46
5	0.176	1.89	-11.4
10	0.361	0.956	-2.08
50	0.66	-0.63	13.29
100	0.74	-0.6	13.17

Table 2: Fluid flow parameters at different temperatures

Temperature °*C*	Diffusivity m^2/s	Viscosity $Pa-s$
1	1149 x 10^{-13}	1730 x 10^{-6}
10	1532 x 10^{-13}	1306 x 10^{-6}
20	2020 x 10^{-13}	1000 x 10−6
30	2590 x 10^{-13}	797 x 10−6
40	3241 x 10^{-13}	652 x 10−6
50	3968 x 10^{-13}	547 x 10−6
60	4771 x 10^{-13}	467 x 10−6
70	5641 x 10^{-13}	404 x 10−6

In the second part of the study the variation of *G* with temperature for a fixed *Pe* and fixed pore throat size was investigated. Temperature has a significant impact on diffusivity, viscosity and density of the fluid. Table 2 displays the values of the parameters used in this study. Diffusivity in water has a non-linear increase with temperature as reported by [16] and [17]. Changes in viscosity of a fluid modulates the ionic mobility, and subsequently changes the residence time of a walker (mimicking an ion) in a pixel as described in the previous section. The reference viscosity for determining the weighting factor responsible for modulating the transition time is taken as the viscosity at 1°C for this study. As density of water does not vary significantly within the range of temperature concerned, it has been kept fixed at $1000 kg/m^3$.

This part of the study corresponds to the transient case where the concentration of the emerging plume is variable. With elapse of time, the concentration of the emerging plume tends to saturate and steady state distribution is achieved. Figure3 shows the σ variation with temperature for two times of observation, the starting time beginning from the time of injection of the random walkers. The dimensions of the channel considered are w=27, L=80 pixels. The *Pe* was fixed at 2.5. Fluid flow is solved using Navier-Stokes. Random walkers introduced at the inlet are moved as per the TDRW scheme. In view of the huge computer memory required, the constant inlet concentration is maintained at 50. A span of

time is defined, τ, considering the smallest possible time of transition of a walker where $\tau = \Delta x^2/6D_{min}$ and D_{min} refers to the minimum diffusivity value which corresponds to 1°C. The time of observation has be either equal or greater than the minimum time of transition in accordance with the TDRW scheme. Subsequently, the time of observations were fixed as τ and 2τ.

Figure 4 shows a typical concentration profile of the middle vertical slice of the cuboid channel at 30°C and 40°C respectively, after an elapse of time τ since the start of the walker movement. It is evident from the concentration profile that the walker plume has not arrived at the outlet at 30°C, whereas it has reached the outlet at 40°C at time τ. This explains the vastly different σ values at these two temperatures in plot Fig.3 for time τ, which shows that σ for temperature 30°C and below are almost nil. At a higher time of observation 2τ, as the movement of the walkers continues for a longer span of time, the plume is able to wade its way to the outlet at temperature as low as 10°C. However at 1°C, the σ value remains negligible. The plots show that conductivity increases with temperature non-linearly with the injection of the walkers. Temperature influences both the factors diffusivity and mobility, which work jointly in the distribution of the walkers through the system. The plots have two regimes clearly similar to output characteristics of CE mode transistor. Comparison of the slopes of the linear regime of the plots reveal that the rate of increase in σ declines with time elapse (Table 3). Consequently, it can inferred that after significant time elapses since injection, the system will arrive at the steady state and the conductivity should linearly increase with temperature.

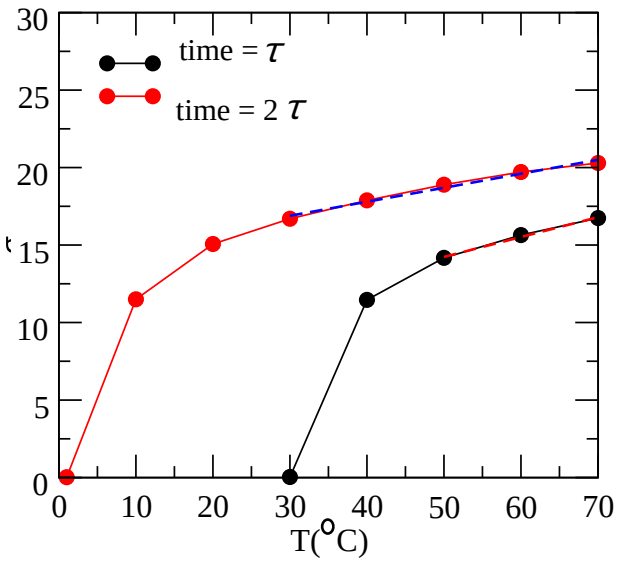

Figure 3: Conductivity at different temperatures through a channel of w=27 pixels and L=80 pixels at *Pe*= 2.5. Time of observations : τ and 2τ. Dotted lines show the linear regime of the non-linear plots.

Table 3: Linear regime of the σ plots

Time elapsed	slope	intercept on σ axis
τ	0.13	7.81
2τ	0.09	14.18

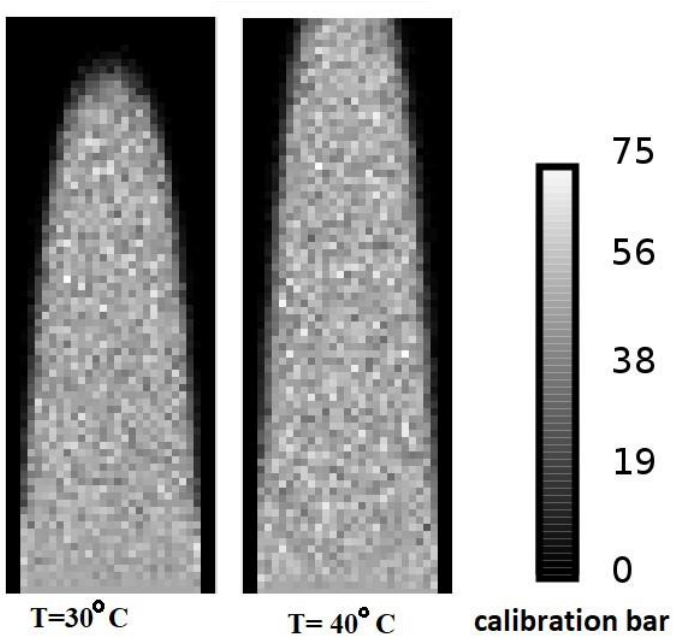

Figure 4: The concentration profile along the middle vertical slice of the sample at temperatures 30°C and 40°C. Time of observation since the start of injection of ions is τ. The adjacent calibration bar shows the concentration of ions associated with the grey shade.

4 Conclusion

The role of *Pe* and temperature in electrical conductivity of fluid filled straight channels in 3-d have been investigated via simulation.

Pore throats of different sizes and equal lengths have been considered which is mode of varying porosity ϕ.

- Conductance (G) increases quadratically with porosity (ϕ) in steady state for all ranges of Peclet number (Pe) considered.
- Conductivity (σ) remains constant with porosity for each *Pe*, but increases with *Pe*. The rate of increase in σ decreases with *Pe*.
- Conductance (G) and thereby conductivity (σ) increase non-linearly with temperature in the transient case.
- A threshold temperature exists corresponding to the time elapsed since the start of injection beyond which the sample starts conducting. • Given any temperature, conductivity increases with the time of observation.
- In the linear regime, conductivity increases steadily with temperature, however, the rate of increase declines with the time elapsed.

References

[1] Hansen D.A., MacDougall R. E., Jacobs J. A., Strangway,D. W., Smellie, D.W., Henderson, R. G., Zietz,I., Gay, S.P., Wilson, A., Andreasen, G.E., Oldham,C.H.G.: Mining Geophysics,Volume II, Theory. Society of Exploration Geophysicists (1967). DOI: https://doi.org/10.1190/1.9781560802716

[2] Rivero OG (1977) Some Considerations About the Possible Use of the Parameters a and as a Formation Evaluation Tool Through Well Logs SPWLA 18th Annual Logging Symposium. Texas June 1977, Houston

[3] Salem HS (1993) Derivation of the Cementation Factor (Archie's Exponent) and the Kozeny-Carman Constant From Well Log Data and Their Dependence on Lithology and Other Physical Parameters. SPE 26309

[4] Bourlange S, Henry P, Moore JC, Mikada H, Klaus A (2003) Fracture porosity in the d´ecollement zone of Nankai accretionary wedge using logging while drilling resistivity data. Earth Planet Sci Lett 209: 103-112

[5] Swanson RD, Singha K, Day-Lewis FD, Binley A, Keating K, Haggerty R (2012) Direct geoelectrical evidence of mass transfer at the laboratory scale. Water Resour Res 48:W10543

[6] Ye YX, Hu XY, Xu D (2015) A goal-oriented adaptive finite element method for 3D resistivity modeling using dual-error weighting approach.J Earth Sci 26:821-826

[7] Singha K, Gorelick SM (2006b) Hydrogeophysical tracking of three-dimensional tracer migration: the concept and application of apparent petrophysical relations. Water Resour Res 42:W06422

[8] Thompson AH, Katz AJ, Krohn CE (1987) The microgeometry and transport properties of sedimentary rock. Adv Phys 36:625-694

[9] Sahimi M (2011) Flow and Transport in Porous Media and Fractured Rock: From Classical Methods to Modern Approaches, 2nd ed. John Wiley and Sons,Weinheim

[10] Dalla E, Cassiani G, Brovelli A, Pitea D (2004) Electrical conductivity of unsaturated porous media: pore-scale model and comparison with laboratory data. Geophys Res Lett 31: L05609

[11] Knudsen HA, Fazekas S (2006) Robust algorithm for random resistor networks using hierarchical domain structure. J Comput Phys 211: 700-718

[12] Aziz,K., Settari,A.: Petroleum Reservoir Simulation. Applied Science Publishers Ltd., London (1972)

[13] Sarkar,S., Toksoz,M.N., Burns,D.R.: Fluid Flow Modelling in Fractures. MIT Earth Resources Laboratory Industry Consortium Meeting, Cambridge (2004)

[14] Dentz, M., Gouze,P., Russian,A., Dweik,J., Delay,F.: Diffusion and trapping in heterogeneous media: an inhomogeneous continuous time random walk approach. Adv. Water Resour. 49,13-22 (2012)

[15] Sadhukhan, S.,Dutta T.: Existence of convective threshold and its role on temperature in reactive flow through fractured rocks: a simulation study in 2D. J. Phys. Commun. 2, 045033 (2018)

[16] Mills, R.: Self-diffusion in normal and heavy water in the range 1–45°. The Journal of Physical Chemistry, 77(5), 685–688 (1973). DOI: 10.1021/j100624a025

[17] Easteal, A.J.,Price, W.E., Woolf, L.A.: Diaphragm cell for high-temperature diffusion measurements. Journal of the Chemical Society: Faraday Transactions 1(85), 1091–1097 (1989). DOI: 10.1039/F19898501091

Received: 14.05.2018
Accepted: 07.06.2018